

Ferroelectric Phase Transitions from First Principles

K. M. Rabe and U. V. Waghmare
Department of Applied Physics
Yale University
New Haven, CT 06520

Abstract

An effective Hamiltonian for the ferroelectric transition in $PbTiO_3$ is constructed from first-principles density-functional-theory total-energy and linear-response calculations through the use of a localized, symmetrized basis set of “lattice Wannier functions.” Preliminary results of Monte Carlo simulations for this system show a first-order cubic-tetragonal transition at 660 K. The involvement of the Pb atom in the lattice instability and the coupling of local distortions to strain are found to be particularly important in producing the behavior characteristic of the $PbTiO_3$ transition. A tentative explanation for the presence of local distortions experimentally observed above T_c is suggested. Further applications of this method to a variety of systems and structures are proposed for first-principles study of finite-temperature structural properties in individual materials.

Presented at the Third Williamsburg Workshop on Fundamental Experiments in Ferro-electrics, February 1995.

1. Introduction

Structural phase transitions in perovskite structure compounds have long been of experimental and theoretical interest [1]. This class of materials exhibits a wide variety of transition behavior and low temperature distorted structures, depending on the individual compound. From first-principles calculations, quantitative information on the structural energetics can be obtained to understand these chemical trends. Furthermore, this approach yields a microscopic description of the origin and nature of lattice instabilities in these materials.

Success in applying the first-principles approach to perovskite oxides has been achieved only rather recently, due to the presence of oxygen and transition metal elements, the number of atoms in the unit cell, and the high accuracy required for a meaningful computation of the delicate lattice instabilities. The 1992 LAPW study [2] of $BaTiO_3$ and $PbTiO_3$ has been followed by investigations in a number of systems using various implementations of density-functional-theory (DFT) methods [3] [4] [5] [6] [7] [8] [9]. In this work, we combine total energy and electronic bandstructure calculations with the DFT perturbation method [10] [11] [12] [13]. The latter provides a means for computing force constant matrices at arbitrary wavevectors \vec{q} without the need for supercells, thus facilitating the exploration of lattice instabilities throughout the first Brillouin zone. Furthermore, valuable information about polarization density in these systems can be obtained from direct computation of the Born effective charge tensors and electronic dielectric constant ϵ_∞ .

The highly demanding nature of these computations has the consequence that direct molecular dynamics or Monte Carlo simulations of temperature-driven structural transitions in perovskite oxides using DFT forces and total energies is completely impractical. Indeed, the investigations mentioned above do not attempt to map out a full configurational energy surface, but rather focus on those aspects felt to be most relevant to the description of the structural transitions: (i) lattice instabilities at quadratic order; (ii) anharmonicity at $\vec{q} = 0$; and (iii) coupling of unstable modes to strain. We have developed a method based on the construction of a “lattice Wannier function” basis [14] which uses this first-principles information for an individual material efficiently to derive an effective Hamiltonian in the low-energy subspace of the ionic displacement space relevant to the temperature range of the transition. This effective Hamiltonian can be regarded as a realistic generalization of the Φ^4 models that are widely used in studies of generic ferroelectric transition behavior [15] [16] [17]. A Monte Carlo simulation of this effective Hamiltonian,

by construction, will quantitatively reproduce the $T \neq 0$ behavior of the particular system under consideration.

To illustrate this approach, we present preliminary results of its application to the ferroelectric transition in $PbTiO_3$. This compound has the cubic perovskite structure at high temperatures, undergoing a first-order transition at 763 K to a tetragonal phase produced by relative displacement of the cationic and oxygen sublattices resulting in a nonzero uniform polarization density. In the first-principles study of this transition, we obtain results for the transition temperature, the order of the transition and the nature of the paraelectric phase. The role of different contributions to the effective Hamiltonian, such as strain coupling and the \vec{q} dependence of the lattice instability, can be examined. The significant differences from $BaTiO_3$ [18] and $SrTiO_3$ [19] become evident. Although $PbTiO_3$ has been described as a “textbook example of a displacive ferroelectric transition,” [1] recent experimental evidence and our first-principles results suggest that the apparent simplicity of this behavior is quite nontrivial.

2. Derivation of the Effective Hamiltonian

The derivation of the effective Hamiltonian [14] is here summarized briefly. The starting point of the analysis is the classical partition function

$$Z \propto \int \{d\vec{u}_j\} \exp(-\beta \mathcal{H}_{lat}(\{\vec{u}_j\})) \quad (2.1)$$

where, as a result of the Born-Oppenheimer approximation, only the ionic degrees of freedom $\{\vec{u}_j\}$ appear explicitly, the index j running over all ions in the system. The Taylor expansion of the full lattice Hamiltonian around a high-symmetry reference structure, such as the cubic perovskite structure, can be grouped into the harmonic terms \mathcal{H}_h and higher-order terms in the displacements \mathcal{H}_{anh} . Diagonalization of the harmonic part \mathcal{H}_h is straightforward, and the results can be depicted using the dispersion relation of the type shown in fig. 1. This suggests a natural decomposition of the full ionic displacement space into two subspaces: (i) Λ_0 , composed of the branches of the dispersion relation that contain unstable modes characteristic of the structural transition, and (ii) Λ_s , composed of the remaining branches, for which typically all modes have $\omega^2(\vec{q}) \geq 0$. This decomposition permits the following approximation to the lattice Hamiltonian:

$$\mathcal{H}_{lat} \approx \mathcal{H}_h(\Lambda_0) + \mathcal{H}_{anh}(\Lambda_0) + \mathcal{H}_h(\Lambda_s) \quad (2.2)$$

where only the anharmonic terms in the unstable subspace Λ_0 , crucial for stabilizing the crystal, are included. As a result, the Λ_s integral in the partition function becomes trivial, making no contribution to the temperature dependence of the average structure, and the partition function reduces to $Z \approx \int_{\Lambda_0} \exp(-\beta \mathcal{H}_{eff}(\Lambda_0))$ where $\mathcal{H}_{eff}(\Lambda_0) \equiv \mathcal{H}_h(\Lambda_0) + \mathcal{H}_{anh}(\Lambda_0)$.

An explicit form for the effective Hamiltonian $\mathcal{H}_{eff}(\Lambda_0)$ is obtained by making a Taylor expansion in coordinates of the subspace Λ_0 . The simplicity of this expression can be maximized by a proper choice of the corresponding basis. In analogy to the tight-binding representation of a subset of electronic eigenstates in a crystal, we choose a highly symmetric localized basis for Λ_0 , where each basis vector $w_{i\lambda}$ is associated with a Wyckoff position in the unit cell \vec{R}_i and transforms according to an irreducible representation of its site symmetry group, the Wyckoff positions and irreps being determined by the space group irrep labels of Λ_0 . These localized basis functions can be related to the Bloch vectors $e_{\vec{q}\lambda}$, which diagonalize $\mathcal{H}_h(\Lambda_0)$, through an expression of the form $w_{i\lambda} = \sum_{\vec{q}} e^{i\vec{q}\cdot\vec{R}_i} e_{\vec{q}\lambda}$ and, by analogy with the electronic case, are given the name ‘‘lattice Wannier functions.’’ With this basis, an ionic configuration in the subspace Λ_0 can be specified by the corresponding coordinates $\{\xi_{i\lambda}\}$.

3. Effective Hamiltonian for $PbTiO_3$

The first-principles method for the construction of the effective Hamiltonian for an individual material proceeds by the following steps. (1) The subspace Λ_0 is identified, a symmetry analysis performed, and approximate Wannier basis vectors constructed by fitting to force-constant matrix eigenvectors at high-symmetry \vec{q} -points. (2) The form for the effective Hamiltonian is obtained by a Taylor expansion in symmetry-invariant combinations of the Wannier coordinates $\{\xi_{i\lambda}\}$. The expansion is truncated to include a relatively small number of physically important terms. (3) Finally, the set of parameters is determined from first principles by fitting \mathcal{H}_{eff} to the results of selected total energy and linear response calculations, using the explicit correspondence, obtained from the construction in step (1), between the Wannier coordinate description $\{\xi_{i\lambda}\}$ and the actual ionic displacements $\{\vec{u}_j\}$. For each material, overdetermination of the parameters through additional independent first-principles calculations is recommended to establish the validity of the truncations made in step (2).

3.1. Construction of Wannier basis

The relevant mode for the ferroelectric transition in $PbTiO_3$, which freezes in to produce the low-temperature tetragonal structure, is the three-fold degenerate zone-center Γ_{15} mode. For a complete identification of the unstable subspace Λ_0 , DFT linear response calculations were carried out at Γ , R , X and M (in the Brillouin zone of the simple cubic lattice) [20]. The resulting low energy eigenmodes Γ_{15} , R_{15} , X'_5 , M'_2 and M'_5 require that the Wannier basis vectors $w_{i\lambda}$, $\lambda = 1, 2, 3$ are situated at the Wyckoff position occupied by the Pb atom and transform according to the vector irrep of the site symmetry group O_h . This results from the significant involvement of the Pb atom in the lattice instability [21] and deviates from what would be expected if the transition could be viewed as resulting from the ‘‘rattling’’ Ti ion picture developed by Slater for $BaTiO_3$ [22], in which case the Wannier basis vectors would be situated at the Ti atom positions.

Following the procedure described in detail in Ref. [14], the Wannier basis vectors are parametrized by identifying the displacement patterns centered at the Pb atoms which transform according to the vector irrep of O_h , starting from the innermost coordination shells. In the present construction, we include displacements of the central, first and second neighbor Pb ions and the nearest Ti and O shells, for a total of nine parameters (fig. 2). The values obtained by fitting to the normalized eigenvectors calculated at Γ_{15} , R_{15} , M'_2 and M'_5 show a rapid decay with increasing distance from the central atom, as expected. Furthermore, the X'_5 eigenvector predicted from the parameters obtained from the fit at the other high-symmetry points is in excellent agreement with the normalized X'_5 eigenvector calculated from first principles. The results are given in detail in Ref. [20].

3.2. Form of the effective Hamiltonian

With this choice of basis, the system is described as a set of three-dimensional vectors $\{\vec{\xi}_i\}$ at the sites of a simple cubic lattice, and \mathcal{H}_{eff} is expanded in symmetry-invariant combinations with respect to O_h^1 , the space group of the cubic perovskite structure. In the present work, intercell interactions are included up to quadratic order only. For first, second and third neighbors, the most general quadratic interactions allowed by symmetry are included:

$$\sum_i \sum_{\hat{d}=nn1} [a_L(\vec{\xi}_i \cdot \hat{d})(\vec{\xi}_i(\hat{d}) \cdot \hat{d}) + a_T(\vec{\xi}_i \cdot \vec{\xi}_i(\hat{d}) - (\vec{\xi}_i \cdot \hat{d})(\vec{\xi}_i(\hat{d}) \cdot \hat{d}))] \quad (3.1)$$

$$+ \sum_i \sum_{\hat{d}=nn2} [b_L(\vec{\xi}_i \cdot \hat{d})(\vec{\xi}_i(\hat{d}) \cdot \hat{d}) + b_{T1}(\vec{\xi}_i \cdot \hat{d}_1)(\vec{\xi}_i(\hat{d}) \cdot \hat{d}_1) + b_{T2}(\vec{\xi}_i \cdot \hat{d}_2)(\vec{\xi}_i(\hat{d}) \cdot \hat{d}_2)] \quad (3.2)$$

$$+ \sum_i \sum_{\hat{d}=nn3} [c_L(\vec{\xi}_i \cdot \hat{d})(\vec{\xi}_i(\hat{d}) \cdot \hat{d}) + c_T(\vec{\xi}_i \cdot \vec{\xi}_i(\hat{d}) - (\vec{\xi}_i \cdot \hat{d})(\vec{\xi}_i(\hat{d}) \cdot \hat{d}))], \quad (3.3)$$

while beyond third neighbor we use a dipole-dipole form parametrized by the mode effective charge \bar{Z}^* and the electronic dielectric constant ϵ_∞ :

$$\sum_i \sum_{\vec{d}} \frac{(\bar{Z}^*)^2}{\epsilon_\infty} \frac{(\vec{\xi}_i \cdot \vec{\xi}_i(\hat{d}) - 3(\vec{\xi}_i \cdot \hat{d})(\vec{\xi}_i(\hat{d}) \cdot \hat{d}))}{|\vec{d}|^3}. \quad (3.4)$$

Terms in the onsite potential, depending only on values of $\vec{\xi}_i$ at a single i , include isotropic terms up to eighth order in $|\vec{\xi}_i|$ and full cubic anisotropy at fourth order:

$$\sum_i (A|\vec{\xi}_i|^2 + B|\vec{\xi}_i|^4 + C(\xi_{ix}^4 + \xi_{iy}^4 + \xi_{iz}^4) + D|\vec{\xi}_i|^6 + E|\vec{\xi}_i|^8). \quad (3.5)$$

The energy associated with homogeneous strain, specified by the tensor $e_{\alpha\beta}$, ($\alpha, \beta = x, y, z$), and its coupling to the local distortion $\vec{\xi}_i$, is included to lowest nontrivial order:

$$\begin{aligned} & + \frac{N}{2} C_{11} \sum_{\alpha} e_{\alpha\alpha}^2 + \frac{N}{2} C_{12} \sum_{\alpha \neq \beta} e_{\alpha\alpha} e_{\beta\beta} + \frac{N}{4} C_{44} \sum_{\alpha \neq \beta} e_{\alpha\beta}^2 + Nf \sum_{\alpha} e_{\alpha\alpha} \\ & + g_0 \left(\sum_{\alpha} e_{\alpha\alpha} \right) \sum_i |\vec{\xi}_i|^2 + g_1 \sum_{\alpha} (e_{\alpha\alpha} \sum_i \xi_{i\alpha}^2) + g_2 \sum_{\alpha < \beta} e_{\alpha\beta} \sum_i \xi_{i\alpha} \xi_{i\beta} \end{aligned}$$

For our calculations in $PbTiO_3$, we take $e_{\alpha\beta} = 0$ at $a_0 = 3.96883 \text{ \AA}$, the lattice constant measured for the cubic phase just above T_c . We have further generalized this expression to include inhomogeneous strain by expanding the effective Hamiltonian subspace according to the procedure described in [14]. The explicit expression is given in [20].

3.3. Determination of parameters from first principles

With the truncations described in the previous section, the effective Hamiltonian for $PbTiO_3$ contains a total of 21 parameters to be determined from first-principles calculations. These are performed with the preconditioned conjugate-gradients plane-wave pseudopotential method, using the program CASTEP 2.1 [23], and with the variational DFT perturbation method, using a program based on the formalism in [11]. Full details of the calculations are provided elsewhere [20].

The determination of the quadratic coupling parameters is greatly facilitated by the use of the DFT perturbation method for the direct calculation of force constant matrices at arbitrary \vec{q} , circumventing the need for computationally intensive supercell calculations. In addition, this method can be used for the direct calculation of Born effective charges Z^* and the dielectric constant ϵ_∞ , from which the dipole-dipole term in \mathcal{H}_{eff} is immediately obtained. At a given \vec{q} , the energies of the three eigenvectors of the quadratic part of the effective Hamiltonian are obtained by computing the quadratic part of the first-principles total energy of the ionic displacement patterns in the Λ_0 subspace from the DFT force constants at that \vec{q} . The eight short-range intercell interactions a_L , a_T , b_L , b_{T1} , b_{T2} , c_L and c_T are then obtained by requiring that the expressions for the effective Hamiltonian eigenenergies in terms of Z^* , ϵ_∞ and the short range intercell interactions reproduce these first-principles values for selected modes at a set of \vec{q} . This process is illustrated in fig. 3. The validity of the dipole-dipole form for intercell interactions beyond third neighbor can be examined by comparing the values predicted by \mathcal{H}_{eff} for calculated energies not included in the determination of the parameters. In fig. 3, these comparisons for \vec{q} along (111) are shown to be very good.

Given the quadratic coupling parameters, the higher order terms in the onsite potential (B , C , D and E), the elastic constants (C_{11} , C_{12} and C_{44}) and the couplings between strain and local distortions (g_0 , g_1 and g_2) can be readily determined from the energies of configurations in which $\vec{\xi}_i$ is independent of i , requiring only total energy calculations for primitive unit cells containing five atoms. Further details of this procedure and the complete set of numerical parameter values for the $PbTiO_3$ effective Hamiltonian are given in [20].

4. Monte Carlo Study of the $PbTiO_3$ transition

The form of the effective Hamiltonian, while greatly simplified relative to the original lattice Hamiltonian, is still sufficiently complicated to discourage the application of analytical statistical mechanics methods such as renormalization group analysis or high-temperature expansions. However, it is quite suitable for Monte Carlo simulation, since changes in energy with configuration are readily calculated numerically [24]. We use a single-flip Metropolis approach, with runs ranging between 25,000 and 150,000 sweeps through the lattice. Periodic boundary conditions are imposed on an $L \times L \times L$ simulation cell, with finite-size scaling applied for L ranging from 5 to 11.

In a finite-size simulation, a first-order transition such as the ferroelectric transition in $PbTiO_3$ leads to the coexistence of two distinct phases, separated by an energy barrier, in a temperature range near T_c . Recently developed Monte Carlo methods for first-order transitions [25] determine the transition temperature from the condition that the difference in the free energies of the two phases be zero. If the two phases are sampled ergodically in the simulation, this difference is quite easy to compute. However, in cases of strongly first-order transitions, unbiased sampling of the two phases can be extremely difficult to achieve, especially as the simulation-cell size increases. While we are presently considering various algorithms suitable for this situation, for now we put bounds on T_c by monitoring the sensitivity of the average structural parameters to the choice of initial state: $T_>$ is the lowest temperature at which the system averages are characteristic of the cubic state, starting with an initial ground state tetragonal configuration, while $T_<$ is the highest temperature at which a starting cubic configuration results in a tetragonal state. These bounds are plotted in fig. 4. A value of $T_c = 660K$, obtained from averaging the bounds at the largest system size, is in very good agreement with the experimental transition temperature 763K. An estimate of a latent heat of 3400 J/mol, extracted from separate runs for the two phases, obtained by using different initial states at T_c , is in rough agreement with the measured value of 4800 J/mol [26], and very much larger than the 209 J/mol latent heat of the cubic-tetragonal transition in $BaTiO_3$ [27].

One of the opportunities offered by this first-principles analysis is to investigate the role of different contributions in determining the behavior at the transition. One particularly striking result of this procedure is that if the strain coupling parameters g_0 , g_1 and g_2 are set to zero, the character of the transition changes significantly. Specifically, the system is then found to undergo a *second-order* transition from the high-temperature cubic phase to a low-temperature *rhombohedral* phase with a lower transition temperature of 400K. Thus, not only is the strain coupling responsible for stabilizing the ground-state tetragonal structure, as has been previously noted [2], but it is also the key factor in producing the strong first-order character of the transition.

Another advantage of computer simulation of a realistic first-principles model is access to microscopic information about short-range order. This is particularly of interest for the high-temperature paraelectric phase. A microscopically nonpolar character for this phase, where the probability distribution of local distortions has a single peak centered at zero, is generally associated with a displacive nature for the transition. In general, a single-well potential will result in a single-peak distribution if intercell correlations are unimportant,

as in the limit of high temperatures. A connection between a single-well onsite potential and displacive behavior has been further supported by a dynamical study of a Φ^4 model [17].

At first glance, the situation in $PbTiO_3$ appears to be straightforward. The onsite potential has a single-well character (positive quadratic coefficient in (3.5)), which by the above arguments seems to explain the reported displacive character of the $PbTiO_3$ transition [1]. However, there is recent evidence that this transition cannot be simply described as displacive. Recent EXAFS measurements [28] show that local distortions, characteristic of the low-temperature structure, persist at least as high as 85K above T_c . In our theoretical approach, we can suggest a possible explanation. In the realistic H_{eff} , unlike the Φ^4 model, we find that unstable modes of the perovskite structure extend all the way to the zone boundary (fig. 3). The associated lowering of the energy for local distortions, even in the absence of long range order, could significantly affect the short-range order above T_c . This feature, rather than the sign of the quadratic coefficient in the onsite potential, may be the signature of a microscopically polar paraelectric phase. More detailed Monte Carlo simulations, including the effective Hamiltonian generalized to include inhomogeneous strain, are in progress. In addition, effective-Hamiltonian molecular dynamics studies are planned which could reconcile large local distortions with the observed “displacive” behavior of the soft mode above T_c .

5. Further applications

The lattice Wannier function method for the construction of effective Hamiltonians is applicable to finite-temperature structural properties in a variety of systems. Effective Hamiltonian studies of structural phase transitions currently in progress include the anti-ferroelectric transition in $PbZrO_3$ [29], the ferroelectric transition in $KNbO_3$ [30], and the cubic-tetragonal transition in ZrO_2 [31]. Effective Hamiltonians can also be constructed to model the temperature dependence of structural parameters in systems like pyroelectric BeO [32]. Because of the simplicity of the kinetic energy in a Wannier basis constructed from the dynamical matrix eigenvectors, this approach is readily extended beyond the equilibrium classical statistical mechanics analysis we have presented here. For example, it is straightforward to construct a quantum mechanical model, for example, for a quantum paraelectric such as $SrTiO_3$ [33]. In addition, important issues in the dynamical properties of ferroelectrics, such as soft-mode behavior and switching, can be studied in molecular dynamics simulations for individual materials.

6. Summary and Conclusions

In conclusion, we have described a systematic method for the construction of effective lattice Hamiltonians from first-principles calculations through the use of a localized, symmetrized basis set of “lattice Wannier functions.” Applying this method to the ferroelectric transition in $PbTiO_3$, we find a first order cubic-tetragonal transition at 660 K. The involvement of the Pb atom in the lattice instability and the coupling of local distortions to strain are found to be particularly important in producing the behavior characteristic of the $PbTiO_3$ transition. A tentative explanation for the presence of local distortions experimentally observed above T_c is suggested. Further applications of this method to a variety of systems and structures are proposed for first-principles study of finite-temperature structural properties in individual materials.

Acknowledgments

We are grateful for useful discussions with Volker Heine, Ronald Cohen, Henry Krakauer, Rici Yu, Cheng-Zhang Wang, Ekhard Salje, Clive Randall, Weiqing Zhong and David Vanderbilt. We thank M. C. Payne and V. Milman for the use of and valuable assistance with CASTEP 2.1. This work was supported by ONR Grant N00014-91-J-1247. In addition, K. M. R. acknowledges the support of the Clare Boothe Luce Fund and the Alfred P. Sloan Foundation.

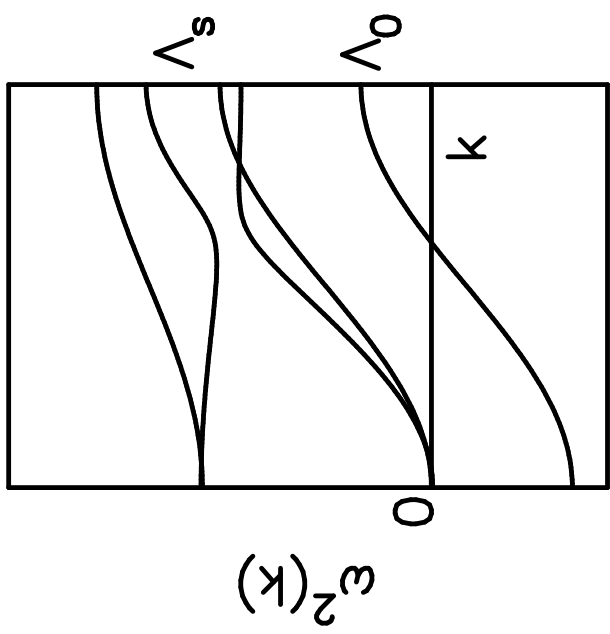
References

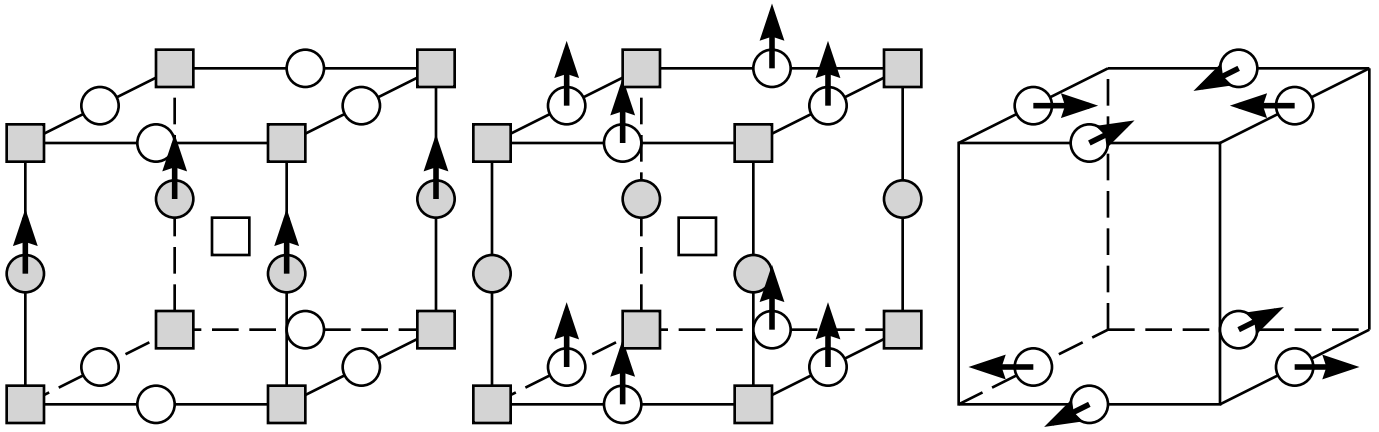
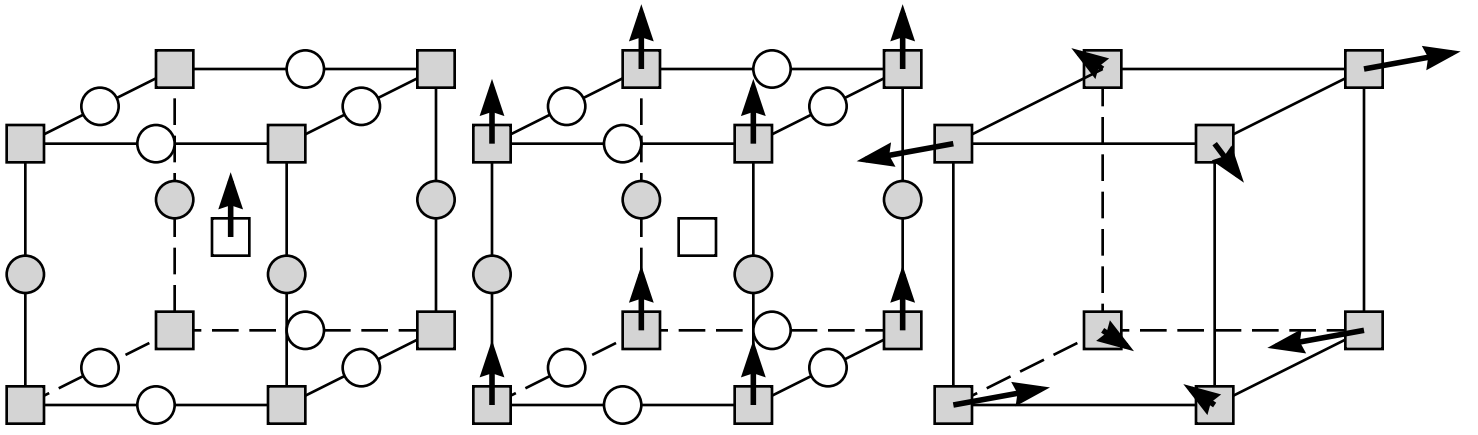
- [1] M. E. Lines and A. M. Glass, *Principles and Applications of Ferroelectrics and Related Materials* (Oxford, 1977), Chap. 8.
- [2] R. E. Cohen and H. Krakauer, *Ferroelectrics* **136**, 65 (1992); R. E. Cohen, *Nature* **358**, 136 (1992).
- [3] R. D. King-Smith and D. Vanderbilt, *Phys. Rev.* **B49**, 5828 (1994); W. Zhong, R. D. King-Smith and D. Vanderbilt, *Phys. Rev. Lett.* **72**, 3618 (1994).
- [4] D. J. Singh and L. L. Boyer, *Ferroelectrics* **136**, 95 (1992).
- [5] K. M. Rabe and U. V. Waghmare, *Ferroelectrics* **151**, 59 (1994).
- [6] M. Posternak, R. Resta and A. Baldereschi, *Phys. Rev.* **B50**, 8911 (1994).
- [7] Ph. Ghosez, X. Gonze and J.-P. Michenaud, *Ferroelectrics* **153**, 19 (1994).
- [8] A. V. Postnikov, T. Neumann and G. Borstel, *Phys. Rev.* **B50**, 758 (1994); A. V. Postnikov and G. Borstel, *Phys. Rev.* **B50**, 16403 (1994).
- [9] H. Krakauer and R. Yu, to be published in *Phys. Rev. Lett.*
- [10] S. Baroni, P. Giannozzi and A. Testa, *Phys. Rev. Lett.* **58**, 1861 (1987); P. Giannozzi, S. de Gironcoli, P. Pavone and S. Baroni, *Phys. Rev.* **B43**, 7231 (1991).
- [11] X. Gonze, D. C. Allan and M. P. Teter, *Phys. Rev. Lett.* **68**, 3603 (1992).
- [12] U. V. Waghmare, V. Milman and K. M. Rabe, unpublished.
- [13] C. Z. Wang, R. Yu and H. Krakauer, *Phys. Rev. Lett.* **72**, 368 (1994); R. Yu and H. Krakauer, *Phys. Rev.* **B49**, 4467 (1994).
- [14] K. M. Rabe and U. V. Waghmare, mtrl-th 9411006.
- [15] S. Fahy and R. Merlin, *Phys. Rev. Lett.* **73**, 1122 (1994).
- [16] A. P. Giddy, M. T. Dove and V. Heine, *J. Phys. Cond. Matt.* **1**, 8327 (1989); B. G. A. Normand, A. P. Giddy, M. T. Dove and V. Heine, *J. Phys. Cond. Matt.* **2**, 3737 (1990)
- [17] S. Padlewski, A. K. Evans, C. Ayling and V. Heine, *J. Phys. Cond. Matt.* **4**, 4895 (1992).
- [18] W. Zhong, D. Vanderbilt and K. M. Rabe, *Phys. Rev. Lett.* **73**, 1861 (1994); *ibid.*, unpublished.
- [19] W. Zhong and D. Vanderbilt, *Phys. Rev. Lett.* **74**, 2587 (1995).
- [20] K. M. Rabe and U. V. Waghmare, unpublished.
- [21] K. M. Rabe and U. V. Waghmare, *Ferroelectrics* **164**, 15 (1995).
- [22] J. C. Slater, *Phys. Rev.* **78**, 748 (1950).
- [23] M. C. Payne, D. C. Allan, T. A. Arias, M. P. Teter and J. D. Joannopoulos, *Rev. Mod. Phys.* **64**, 1045 (1992).
- [24] M. P. Allen and D. J. Tildesley, *Computer Simulation of Liquids*, (Oxford, 1987), Chap. 4.

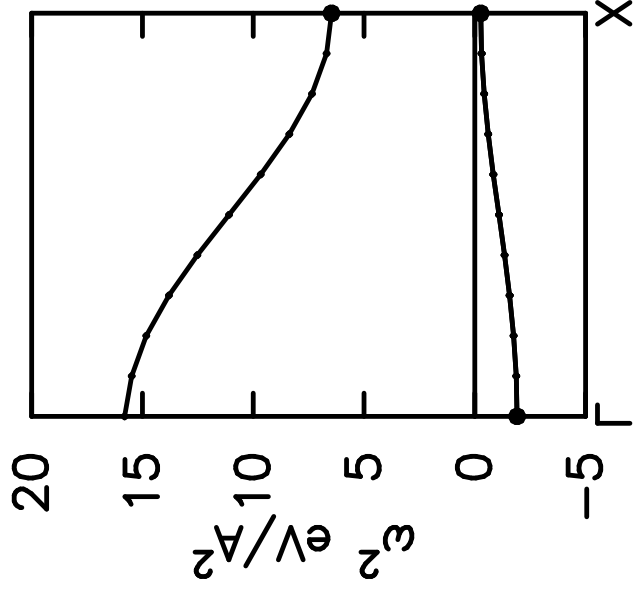
- [25] B. A. Berg and T. Neuhaus, Phys. Rev. Lett. **68**, 9 (1992); C. Borgs and W. Janke, Phys. Rev. Lett. **68**, 1738 (1992); W. Janke, Phys. Rev. **B47**, 14757 (1992).
- [26] G. Shirane and E. Sawaguchi, Phys. Rev. **81**, 458 (1951).
- [27] G. Shirane and A. Takeda, J. Phys. Soc. Jpn. **7**, 1 (1952).
- [28] N. Sicron, B. Ravel, Y. Yacoby, E. A. Stern, F. Dogan and J. J. Rehr, Phys. Rev. **B50**, 13168 (1994).
- [29] U. V. Waghmare and K. M. Rabe, in preparation.
- [30] R. Yu, U. V. Waghmare, H. Krakauer and K. M. Rabe, in preparation.
- [31] R. B. Phillips, U. V. Waghmare, and K. M. Rabe, in preparation.
- [32] B. A. Elliott, U. V. Waghmare and K. M. Rabe, in preparation.
- [33] R. Martonak and E. Tosatti, Phys. Rev. **B49**, 12596 (1994).

Figure Captions

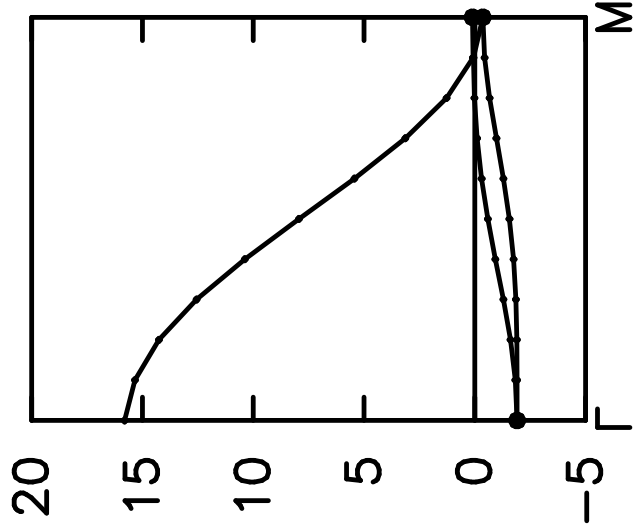
- Fig. 1. A sketch showing the features of the dispersion relation $\omega_\lambda^2(\vec{q})$ characteristic of systems undergoing structural transitions, and a possible decomposition into the two subspaces Λ_s and Λ_0 described in the text.
- Fig. 2. Independent displacement patterns for the innermost coordination shells of the lattice Wannier functions transforming like the \hat{z} vector component at the Pb atom positions. The open squares represent the Pb ions, the shaded squares the Ti ions, and the open and shaded circles represent inequivalent oxygen ions. The three additional displacement patterns for first and second neighbor Pb shells, included in the analysis, are not shown. The \hat{x} - and \hat{y} -like components are obtained by rotating the patterns shown by $\frac{\pi}{2}$ around an appropriate cartesian axis.
- Fig. 3. Determination of quadratic short-range intercell interaction parameters for $PbTiO_3$. The solid and open circles indicate the first-principles values for the energies of effective Hamiltonian eigenvectors. The solid circles are used to determine values for the short-range interaction parameters, which are used to generate the effective Hamiltonian dispersion curves, shown as solid lines. The open circles are first-principles results not included in the parameter determination, for comparison.
- Fig. 4. Monte Carlo estimate of T_c as a function of increasing simulation-cell size L . At each L , the vertical line extends from the lower bound $T_{<}$ to the upper bound $T_{>}$, calculated as described in the text.



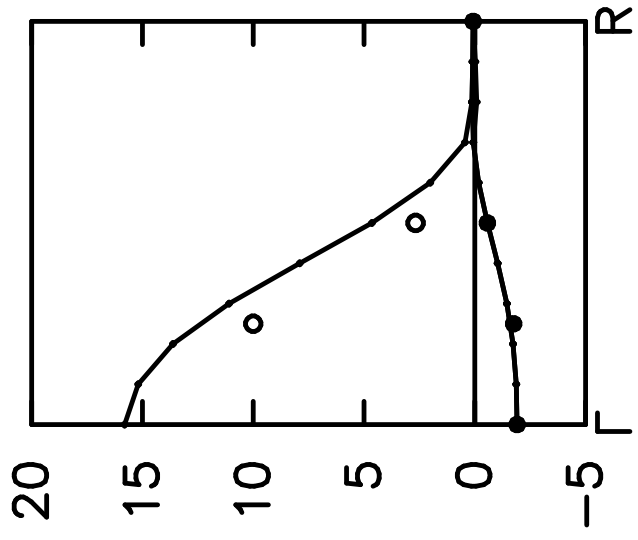




$k(001)$



$k(110)$



$k(111)$

